Effect of Reacting Gas Flowrates and Hydration on the Carbonation of Anion Exchange Membrane Fuel Cells in the Presence of CO₂

Yiwei Zheng¹, Garrett Huang², Lianqin Wang³, John R. Varcoe³, Paul A. Kohl² and W.E. Mustain¹*

¹Department of Chemical Engineering, Swearingen Engineering Center, University of South Carolina, Columbia, SC 29208, United States

²School of Chemical and Biomolecular Engineering, Georgia Institute of Technology, Atlanta, Georgia, USA

³Department of Chemistry, The University of Surrey, Guildford, Surrey GU2

7XH, United Kingdom

*Corresponding author: Email: mustainw@mailbox.sc.edu; Phone: 803-576-6393

Keywords: Anion Exchange Membrane; Fuel Cell; CO2; Carbonate; Air

Abstract

Anion exchange membrane fuel cells (AEMFCs) have been widely touted as a low-cost alternative to existing proton exchange membrane fuel cells. However, one of the limitations of this technology has been the severe performance penalty related to the introduction of CO₂ to the cell – typically in the air cathode feed. Introduction of CO₂ into AEMFCs results in cell carbonation, which can impart thermodynamic, kinetic and Ohmic overpotentials that can add up to hundreds of millivolts. Therefore, it is important to find strategies and operational protocols for AEMFCs that minimize these overpotentials. In this paper, we investigate the impacts of the anode and cathode flowrate, as well as the cell hydration level, on the extent of cell carbonation and cell polarization. Key findings include: (1) decreasing the cathode flowrate generally decreases the total CO₂-related voltage loss while changing the anode flowrate has a minimal effect; (2) increasing cell hydration helps to mitigate the performance loss in the presence of CO₂; and (3) operational combinations are found that significantly reduce the CO₂ penalty compared to the present literature.

1. Introduction

Alkaline-based fuel cells can have advantages over their more popular counterpart, the proton exchange membrane fuel cell (PEMFC). For instance, traditional alkaline fuel cells (AFCs) can be operated with much lower quantities of noble metal catalyst or even with non-noble metal electrocatalysts like nickel, silver, etc.¹ Also, the electrolyte, liquid KOH, is much less expensive than Nafion[®]. For this reason, AFCs are still being pursued by companies such as AFC Energy PLC in the UK.

However, despite their possible cost advantages, AFCs are not being widely implemented today and the primary reason is that the OH⁻ anions in the electrolyte react with CO₂ in the ambient air cathode feed to form (bi)carbonates^{2–4} (Equations 1 and 2).

$$OH^- + CO_2 \leftrightarrow HCO_3^- \tag{1}$$

$$HCO_3^- + OH^- \leftrightarrow CO_3^{2-} + H_2O \tag{2}$$

The resulting CO₃²⁻ anions react with the mobile K⁺ ions in the electrolyte to form the low solubility compound K₂CO₃, which can precipitate onto the cathode electrode. The salt formation lowers the performance and stability of the AFC. Strategies have been proposed to solve this CO₂ poisoning problem. For example, <u>Cifrain</u> and Kordesch⁵ found that the negative effects of CO₂ poisoning can be partly mitigated by circulating the electrolyte. Another possibility is to change the electrolyte from a liquid (aqueous salt solution) to an ion conducting polymer, i.e. by the use of an anion exchange membrane (AEM) – creating so-called anion exchange membrane fuel cells (AEMFCs). AEMFCs avoid salting because the positively charged cations are stationary (typically covalently bound to the polymer backbone) and not alkaline earth

ions, eliminating the possibility for precipitates to form. As a result, the CO_3^{2-} anions are able to be transported through the AEM, and they are able to carry a portion of the charge from the cathode to the anode to complete the electrochemical circuit.^{6,7} However, this does not mean that carbonation has a null effect on AEMFC behavior.

For many years it was very difficult to understand the effects of carbonation on AEMFC behavior due to the chemical instability of available AEMs and very low cell performance. Fortunately, the past few years have seen a significant improvement in both AEM properties and AEMFC performance. For instance, there have been several reports of AEMs with hydroxide conductivity of over 100 mS/cm (60°C to 80°C)^{8–10} and recent reports of AEMs having conductivity over 200 mS/cm (at 80°C). State-of-the-art AEMFCs have the ability to achieve peak power densities over 3 W cm⁻² operating on H₂/O₂ gas feeds⁸. One notable example by Huang et.al reported AEMs made from poly(norbornene) block copolymer with very high hydroxide conductivity, 198 mS/cm, and record peak power density in a hydrogen/oxygen fuel cell, 3.4 W/cm² at 80°C. Also, the performance stability of AEMFCs has improved dramatically during this time, with multiple groups reporting 500+ hour stability at low degradation rates (5 – 10%)^{12–15}.

Now that AEMFC performance and stability have been enhanced to the point where their future deployment in real applications is realistic, it is now an important time in AEMFC development to begin to answer some of the contemporary issues that have to date been mostly put aside in the literature, including operating on real air, which contains CO₂, leading to the carbonation discussed above. Recently, there have

been several experimental $^{16-21}$ and modeling $^{22-25}$ studies that have allowed researchers in the field to well-understand how adding CO_2 to high performing AEMFCs influences their behavior.

There are three primary mechanisms for voltage loss. First, as carbonate anions are formed at the AEMFC cathode from Equations 1 and 2, they migrate through the AEM from the air cathode to the hydrogen anode. Carbonate mobility is lower than hydroxide mobility, which leads to an increase in the area-specific resistance (\triangle ASR). Second, because hydrogen does not react with the carbonate directly at relevant potentials, carbonates are not immediately released on arrival to the anode as CO₂. Instead, there is a time lag while the carbonates accumulate at the anode and the pH of that electrode drops²⁶ – forcing the reverse of Equations 1 and 2 to occur before the CO₂ is eventually released. The drop in the anode pH leads to a thermodynamicallydriven increase in the anode potential (ΔV_{Nernst}), reducing the overall cell voltage. This has been successfully modeled by Gerhardt et. al²³, Krewer et. al²⁴ and Wrubel et. al²⁷. Third, the accumulation of carbonates in the anode causes low local OHconcentrations throughout the anode, leading to an increase in the anode charge transfer This third effect was captured quite well in the Gerhardt resistance, (ΔR_{ctHOR}). model²³. Therefore, the operating voltage for an AEMFC with CO₂ in the cathode feed can be described by Equation 3¹⁶:

$$V_{cell} = V_{OCV} - i \left(R_{\Omega,OH} + R_{ctORR} + R_{mtORR} + R_{ctHOR} \right)$$
$$-\Delta V_{Nernst} - i \left(\Delta ASR + \Delta R_{ctHOR} \right) \quad (3)$$

In total, the voltage loss from these three mechanisms are typically several hundred millivolts under operating conditions of practical interesting. The Nernstian voltage loss (ΔV_{Nernst}) and increase in the charge transfer resistance ($i\Delta R_{ctHOR}$) dominate the CO₂-related performance loss whereas the voltage loss related to the ASR ($i\Delta ASR$) increase is often a minor contributor (< 10% of the total loss) ^{16,23}.

There are several pathways by which the CO₂-related voltage losses can mitigated. In our previous work, 16 it was shown that increasing the AEMFC operating current density and increasing the cell temperature can slightly mitigate the negative effects of CO₂. Lowering the CO₂ concentration in the reacting gas below 400 ppm can also help, but at high cathode flowrates, even having 5 ppm CO₂ in the cathode feed has been untenably harmful, resulting in CO₂-related voltage losses of about 100 mV^{16,23,28}. Therefore, it is important to continue to explore the impact of cell operating conditions on the tolerance of AEMFCs to the presence of CO₂ in the cathode feed. In this study, three new variables are investigated: the anode flowrate, the cathode flowrate, and the cell hydration. The cathode reacting gas flowrate is expected to be important because it sets the total dose of CO2 that is fed to the cell. The anode flowrate can influence the degree of cell carbonation because it will inevitably control the concentration of CO₂ (i.e. via dilution) in the anode stream. The CO₂ in the hydrogen stream, which is usually recirculated, can be taken back up into the cell. Lastly, the level of cell hydration may influence how much CO₂ can be taken up by the cell (i.e. Equations 1 and 2) as well as its overall concentration.

2. Experimental

Electrode Preparation

The electrodes in this work were prepared using a method that has been detailed in our previous publications ^{10,15,29,30}. Briefly, the anode and cathode catalysts were 60 wt% PtRu supported on Vulcan XC-72R (Alfa Aesar HiSPEC 10000, 2:1 ratio of Pt:Ru by mass – Pt nominally 40 wt%, and Ru, nominally 20 wt%) and 40 wt% Pt supported on Vulcan XC-72R (Alfa Aesar HiSPEC 4000, Pt nominally 40 wt%), respectively. Electrode preparation was initiated by placing an ethylene tetrafluoroethylene (ETFE) benzyltrimethylammonium (BTMA) solid powder anion exchange ionomer (AEI, ionexchange capacity IEC = 1.24 mmol g^{-1}) into a mortar and grinding it by hand with a pestle for 10 min. The catalyst powder, Vulcan carbon (XC-72R, Cabot), and 1 mL of Millipore deionized (DI, 18.2 M Ω cm resistivity) water were added to the mortar and ground for an additional 10 min. The mass fraction of AEI in the catalyst layer was always 0.20 and the mass fraction of carbon was maintained at 0.48 for both electrodes. Next, the catalyst-AEI slurry was transferred to a centrifuge tube. Solvent was added and the mixture was sonicated (Fisher Scientific FS30H) for 60 min. The water in the ultrasonic bath was maintained below 5 °C to avoid degrading the supported catalyst and the AEI, and to maximize the electrochemically active area. The ink dispersions were sprayed onto Toray TGP-H-060 gas diffusion layers with 5 wt% PTFE wetproofing with an Iwata Eclipse HP-CS (the carrier gas was 15 psig ultra high purity, UHP, N₂) to create gas diffusion electrodes (GDEs). The target catalyst loading on both the anode and cathode GDEs was 0.6 ± 0.1 mg_{Pt} cm⁻².

Anion Exchange Membrane Fuel Cell (AEMFC) Assembly and Break-in Procedure

Before cell assembly, the GDEs were soaked in 1 M aqueous KOH solutions (made from Fisher Chemical pellets/certified ACS and DI water) for 60 min, exchanging the solution twice during this time. At the same time, the AEM was soaked in an identical solution. After the 1 h soak, excess KOH was removed from the GDEs and AEMs before cell assembly. The GDEs and AEMs were pressed together in the cell to form each membrane electrode assembly (MEA) in situ with no prior hot pressing. The MEAs were loaded into 5 cm² Scribner hardware between two single pass serpentine flow graphite plates. The MEA was sealed and compressed with 6 mil (152 μm) PTFE gaskets with 20% - 25% pinch at 5.1 N·m torque. An 850e Scribner Fuel Cell Test Station was used to control the gas stream dew points, cell temperature, gas flowrates and the operating current density.

Four different AEMS were used in this study. The first was a benzyltrimethyl ammonium-(BTMA)-type radiation-grafted AEM ³¹ made from a 25 μm low density polyethylene (LDPE) precursor film (LDPE-BTMA, IEC = 2.5 mmol g⁻¹), which was used when investigating the influence of flowrate on the CO₂-related voltage losses. The second was an ETFE-BTMA-based radiation-grafted AEM³² (ETFE-BTMA, IEC = 2.1 mmol g⁻¹, 50 μm when fully swollen in water), which was used when probing the effect of hydration on CO₂ uptake at 60 °C. Third, a tetra-block poly(norbornene) (PNB) copolymer with 64 mol% halogenated monomer with different mole percent of cross-linking agent *N,N,N',N'*-tetramethyl-1,6-hexanediamine (TMHDA) were used. The mole percent of TMHDA relative to the number of head-groups was: 5 mol%, 15 mol%

and 25 mol%. These films are denoted as GT-64-X, where X is the crosslinker content. For example, GT-64-5 has 5 mol% TMHDA with respect to the moles of head-group within the copolymer. GT-64-X AEMs were tested to show how AEM water uptake can be tuned to influence cell carbonation. Lastly, a BTMA-functionalized radiation-grafted AEM made from 15 μm high density polyethylene (HDPE-BTMA, IEC = 2.4 mmol g⁻¹)³³ was used for experiments that were trying to find the minimum CO₂-related voltage loss within the operating conditions of this study. The choice of using multiple AEMs was purposeful. First, it shows how widespread the carbonation issue is. Voltage loss upon exposure to CO₂ is not a chemistry-specific phenomenon; it is intrinsic to operation of AEMFCs. Second, there are some physical properties of the various AEMs that are useful to show. For example, some AEMs have poorer stability at high temperature or lower water uptake – though developing an understanding of the explicit effects of membrane physical properties is not attempted here. To be consistent, each variable tested in this work deploys a single AEM.

Before CO₂ measurements were made, all cells underwent a break-in procedure. First, the cell was brought to its operating temperature under N₂ flow on both sides of the cell at 100% relative humidity (RH). Then, the feed gases were switched to UHP H₂ and O₂ (Airgas) at the anode and cathode, respectively. Next, the cell was operated potentiostatically, stepwise from 0.7 V to 0.3 V (0.1 V steps, held for a minimum of 30 min at each step) as the reacting gas dew points were optimized per our standard procedure^{15,29,30}. The optimized reacting gas dew points were very repeatable from cell-to-cell; dew points were typically 50 °C at the anode and 52 °C at the cathode for an

AEMFC operating at 60 °C. Following the optimization of the reacting gas dew points, the cell was operated galvanostatically at 1.0 A cm⁻² and allowed to equilibrate for at least 30 min before CO₂ exposure was initiated. Multiple cells were constructed and tested for each measurement.

AEMFC Carbon Dioxide Measurements

Following the break-in procedure and 30 min equilibration, the cell current was held constant and 400 ppm CO₂ was added to the UHP O₂ cathode stream. CO₂ was added to O₂ in lieu of air in order to simplify observations because air has additional O₂ mass transport impact (e.g. N₂ dilution) during cell operation, which is largely eliminated by utilizing O₂ as the reacting gas. The flowrates for O₂ and H₂ were varied from 0.2 to 1 L min⁻¹. Typically, after CO₂ addition, the cell was operated for 10 min, which was much longer than the time required to reach quasi-steady-state operation (typically < 5 min, though lower CO₂ concentrations took longer to reach steady-state). After 30 min operation at constant current, CO₂ was removed from the gas stream and the cell was allowed to decarbonate for an initial 10 min. After this, the cell was fully decarbonated by lowering the cell potential to 0.1 V for 2 min, after which no CO₂ emission was measured in the anode stream and the operating voltage returned to the value observed before CO2 was added. The concentration of CO2 emitted from the anode and cathode was constantly monitored in real time using a PP Systems WMA-5 non-dispersive infrared CO₂ gas analyzer (a water trap was placed in-line before the WMA-5 in order to preserve the unit and its calibration).

3. Results and Discussion

3.1 Influence of flowrate on AEMFC performance with 400 ppm cathode CO₂

The effect of cathode flowrate (oxygen with 400 ppm CO₂) on the behavior of a carbonated AEMFC is presented in Figure 1. As shown in Figure 1a, the CO₂-related voltage loss decreased (i.e. improved) approximately linearly with decreasing cathode gas flowrate, showing that the total dose of CO₂ fed to the cell plays an important role in carbonation. Additionally, as shown in Table 1, the steady-state carbonation of the AEM and electrode ionomer in the operating cell increased with higher oxidant flowrate. As described in our previous publication, ¹⁶ the carbonate content in the AEMFC can be estimated by first converting the CO₂ concentration vs. time data (Figure 1b) from the anode and cathode exhaust into flux vs. time data (Figure 1c) and then integrating the area under the flux curves for the anode exhaust, cathode exhaust and a "blank". blank is a direct measure of the amount of CO₂ added to the cathode, a measurement that is made in the absence of the anionic polymer. For more information on the "blank" experiment, please see the Supporting Information file. Hence, the amount of carbonate/CO₂ in the cell for any operating condition can be calculated (N_{CO2}) by Equation 4:

$$N_{CO2} = \int$$
 "blank"(t) dt $-\int$ "anode exhaust"(t) dt $-\int$ "cathode exhaust"(t) dt (4)

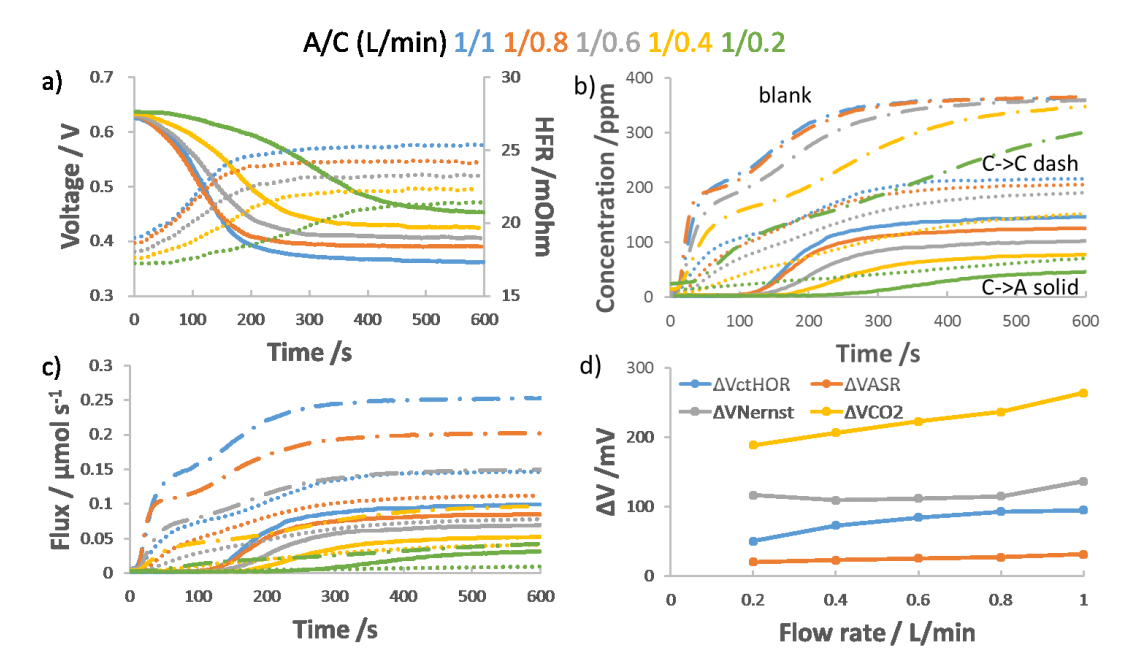


Figure 1. Effect of cathode flowrate on the carbonation of an AEMFC operating at 1 A/cm^2 and $60 \,^{\circ}\text{C}$ with the LDPE-BTMA AEM, 400 ppm CO_2 fed to cathode at t=0 s, 1 L/min anode flowrate, 5cm^2 active area. a) Voltage loss (solid lines) and HFR increase (dotted lines) following the introduction of CO_2 into the cathode; b) Concentration of CO_2 in the anode (solid lines) and cathode (dotted lines) effluent streams; c) CO_2 flux in the anode and cathode effluent; d) deconvoluted CO_2 -related voltage losses. In panels a)-c), the results are color-coded based on flowrate, as indicated at the top of the figure. In panels b) and c), the cathode "blank" plots are shown by combination dash-dot lines.

Table 1. Degree of steady-state carbonation as function of cathode flowrate feeding with 400 ppm CO₂.

Anode/Cathode Flowrate (L/min)	1 /1	1/0.8	1/0.6	1/0.4	1/0.2
AEMFC carbonate N_{CO2} / μ mol	21 ± 3	17 ± 2	13 ± 2	8 ± 2	4 ± 2
Anode carbonate / µmol	8 ± 2	7 ± 2	7 ± 2	8 ± 2	8 ± 2

Evidence for the uptake of CO_2 into the cell is also given by the cell's high frequency resistance (HFR with $ASR \cong HFR \times A$ where A = geometric cell area), shown in Figure 1a. Lower cathode flowrates resulted in a lower HFR. It was also interesting to note that it took a longer time for the cell to reach a stable HFR value and voltage at

a lower flowrate. These dynamics also match well with what was observed with the CO₂ concentration in the anode exhaust, Figure 1b. Even at the same operating current density (same charge flux through the AEM), the CO₂ breakthrough time in the anode exhaust was longer at lower flowrates. This shows that CO₂ accumulation is slower in the AEMFC anode at lower flowrate, that is the flux of carbonate across the cell is lower. The data also shows that the flux of CO₂ leaving the anode (Figure 1c, calculations in the Supporting Information) at steady state is lower at lower flowrate; hence, the rate of CO₂ uptake at the cathode is also less at lower flowrate.

It might be thought that combining the lower rate of anode carbonate accumulation combined with a lower incoming flux would reduce the amount of carbonate in the anode during cell operation. However, the release of CO₂ requires the accumulation carbonates in the anode. Eventually the number of supplied carbonate ions result in a sufficiently high carbonate concentration at the anode such that the reverse of Equations The speciation shifts from CO₃² to HCO₃ and then finally CO₂. 1-2 occurs. Because CO₂ release is always observed at the anode, it is possible that the anode carbonate concentration may not be significantly different across the range of flowrates. To estimate the total amount of carbonate in the anode electrode, the CO₂ was removed from the cathode feed until the cell reached a new steady state. The resulting cell was then pulsed to 0.1 V and the amount of CO₂ in the anode exhaust was measured versus The integral of the CO₂ concentration vs. time can be used as an estimate total time. amount of carbonate left in the cell, which, after the new steady state, should overwhelmingly be in the anode. 16 These values are also reported in Table 1 where it was found that the total amount of anode carbonate was nearly unchanged with cathode flowrate. This effect of AEMFC N_{CO2} vs. total amount of anode carbonate also has implications on the individual contributions to the CO₂-related voltage loss, discussed above. However, before deconvoluting the effect of the cathode flowrate on the root causes for cell voltage loss, it is important to point out from Figure 1b that AEM-like devices can also act as CO₂-separators which can simultaneously generate energy, unlike traditional approaches which consume energy.

Though Figure 1a is informative, data following the release of CO₂ is needed in order to deconvolute the CO₂-related voltage loss into its fundamental constituents: ΔASR , ΔV_{Nernst} and ΔR_{ctHOR} . That raw data is shown in Figure S2 – S6 in the Supporting Information and the quantified values for ΔASR , ΔV_{Nernst} and ΔR_{ctHOR} are presented in Table S1. The details for performing the deconvolution was extensively described and demonstrated elsewhere 16, but a short description and visualized calculation of the decoupling process is provided in the Supporting Information file. Figure 1d graphically display the results of the deconvolution. In Figure 1d, ΔASR increased almost linearly with the cathode flowrate, and the total amount of carbonate in the cell shown in Table 1. ΔR_{ctHOR} increased with flowrate as the amount of carbonate in the cell increased, with the smallest increase at the lowest flowrates. Figure 1d presents ΔV_{Nernst} as a function of cathode flowrate as well as the voltage loss caused by the other two mechanisms, allowing ΔV_{Nernst} , ΔV_{ASR} (ΔV_{ASR} = $i\Delta ASR$) and ΔV_{ctHOR} $(\Delta V_{ctHOR} = i\Delta R_{ctHOR})$ to be compared. Here, the overall voltage loss was dominated by the Nernstian loss and the increase in the charge transfer resistance. It should be noted

that the Nernstian loss was the most significant, and was nearly constant regardless of the flowrate, which agrees well with the anode carbonation state in Table 1. This suggests that the outermost part of the anode, where the potential is measured experimentally, remains firmly dominated by the bicarbonate/CO₂ equilibrium at all flowrates. The next largest contributor to the cell performance loss was the charge transfer resistance. It was also the most affected by flowrate. For completeness, Figure S7 and Table S2 show the cathode flowrate effect with a GT-64-15 AEM as well, which showed the same behavior.

Next, the effect of lowering the anode reacting gas flowrate was investigated and the results are shown in Figure 2. In general, the anode flowrate did not have a significant impact on the CO₂-related overpotential. Figure 2a shows that the CO₂ overpotential only very slightly increased with decreasing H₂ flowrate. This was not due to a significant increase in the amount of carbonate in the system, as evidenced by the similar HFR for all cases and the total cell carbonation being similar (Table 2). This suggests that the main reason for increased polarization is increased carbonate concentration in the anode, particularly right at the anode/GDL interface, which is evidenced by larger Nernstian and charge transfer losses at lower flowrates as well as the semi-quantitative measurement of anode CO₂ content (using the procedure described above for the cathode) as summarized in Table 2.

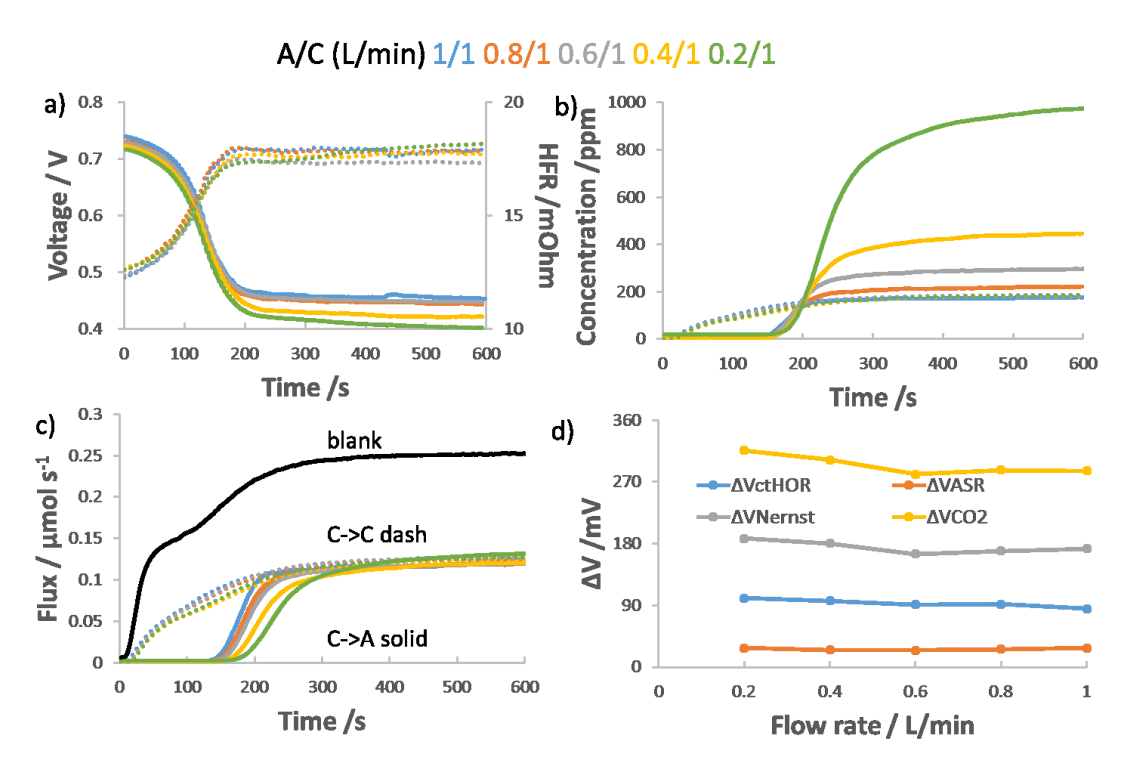


Figure 2 Anode flowrate effect on AEMFC carbonation and performance loss. AEMFC operating at 1 A/cm² and 60 °C with a LDPE-BTMA AEM, 400 ppm CO_2 fed to cathode at t=0 s, 1 L/min anode flowrate, 5 cm² active area. a) Voltage loss (solid lines) and HFR increase (dotted lines) following the introduction of CO_2 into the cathode; b) Concentration of CO_2 in the anode (solid lines) and cathode (dotted lines) effluent streams; c) CO_2 flux leaving the anode and cathode; and d) deconvoluted CO_2 -related voltage losses.

Table 2. Degree of steady-state carbonation as function of anode flowrate feeding with 400 ppm CO₂.

Anode/Cathode Flowrate (L/min)	1 /1	0.8/1	0.6/1	0.4/1	0.2/1
AEMFC carbonate / μmol	19 ± 2	20 ± 2	20 ± 2	27 ± 3	24 ± 4
Anode carbonate / µmol	11 ± 2	11 ± 6	14 ± 4	14 ± 2	18 ± 2

It was observed that as the anode flowrate was decreased, the CO₂ concentration in the anode exhaust increased, which is shown in Figure 2b. In fact, it was possible for the concentration of CO₂ in the anode exhaust to be significantly higher than the CO₂ concentration in the cathode feed, showing that these devices can act as CO₂

ppm CO₂ regardless of the H₂ flowrate, showing that the extent of carbonation near the cathode was very low, and suggesting that the cathode likely sees minimal resistance to CO₂ uptake and carbonate formation. The carbonate uptake and flux across the cell was essentially independent of anode flowrate (Figure 2c) because of the rapid reaction between carbon dioxide and hydroxide. Finally, as described above, the polarization losses were deconvoluted from the data where CO₂ was supplied and removed from the cathode (Figure S8 - S12 in the Supporting information file). As shown in Figure 2d, none of the three major contributors to the CO₂-related overpotential changed significantly as the anode flowrate was changed.

The final flowrate-related experiment involved lowering the flowrates of both the anode and cathode gases simultaneously and equally. As shown in Figure 3a, the voltage and HFR showed similar behavior to Figure 1a as CO₂ is applied. It is noted that the initial operating voltage is different in each case due to performance differences at lower reacting gas flowrates; low flowrates can make it more difficult to manage the AEMFC water production at the anode and this has an effect on the cell performance^{15,29}. In fact, in these cells, stable operation at 0.2 L/s was not possible and is, thus, not reported here. There were some notable CO₂-related cell dynamics at this condition that were not obvious by looking at the data in Figures 1 and 2. For instance, in Figure 3b, the amount of CO₂ in the exhausts were comparable, suggesting a balance between the dosing and removal. In addition, Figure 3c shows higher flux at reasonably higher flowrates. But the most surprising observations were made after

deconvoluting the data sets where CO₂ was first applied and then released (shown in Figure S13 - S15 in the Supporting Information) to determine the contribution of each of the fundamental causes of CO₂-related voltage loss. The Nernstian, Ohmic and kinetic losses from the addition of CO₂ at various identical anode/cathode flowrates are summarized in Figure 3d. Despite the dynamics in the CO₂ flux (Figure 3c) at various flowrates, lowering the flowrates symmetrically did not significantly impact the total CO₂-derived overpotentials nor did it drastically change any individual contributor, though there does seem to be some interplay between ΔR_{ctHOR} and ΔV_{Nernst} where the former slightly increases with flowrate and the latter decreases. This can be understood based on the dynamics of the system where despite the fact that lower cathode flowrates reduce the dosing of the cell, the lower anode flowrate makes it more difficult to remove carbonate from the system. Thus, at lower flowrates, as summarized in Table 3, despite similar overall amounts of carbonate in the system, the anode itself appears to have a higher total amount of CO2 at lower flowrate than at higher flowrate, which is expected to increase the charge transfer resistance. Nernstian voltage loss did slightly increase with decreasing flowrates, which is most likely the result of carbonate accumulation in regions of the cell other than the anode. This causes the pH difference between the anode and cathode to be less at lower flowrates than higher flowrates. Figure S16 and Table S2 show the same flowrate effect with a different membrane, GT-64-15, which again showed the same behavior.

A/C (L/min) 0.8/0.8 0.6/0.6 0.4/0.4 0.7 a) Concentration / ppm 200 0 0.6 **Noltage / N** 0.5 0.4 HFR/mOhm C->C dash C->A solid 0.3 15 300 300 0 200 400 500 600 400 500 Time /s Time /s **c)** 0.25 d) 300 -ΔVctHOR ---ΔVASR ---ΔVNernst -Elax / 0.2 0.15 0.15 0.05 **№** 200 **№** 100 0 0 200 300 100 400 500 600 0.2 0.4 0.6 0.8 1 Time /s Flow rate / L/min

Figure 3. Effect of symmetrically reducing the anode and cathode flowrate on AEMFC carbonation. All cells were operated at 1 A/cm² and 60 °C with 25 um LDPE-BTMA AEM, 5cm² active area. The concentration of CO_2 fed to the cathode was 400 ppm CO_2 applied at t=0 s. a) voltage losses and HFR increases after the introduction of CO_2 , b) CO_2 emission from the anode (solid lines) and cathode (dotted lines); c) CO_2 flux; and d) deconvoluted CO_2 related voltage losses at the investigated symmetrical flowrates.

Table 3. Degree of steady-state carbonation as function of anode/cathode flowrate feeding with 400 ppm CO₂.

Anode/Cathode Flowrate (L/min)	0.8/0.8	0.6/0.6	0.4/0.4	
AEMFC carbonate/ μmol	15 ± 4	14 ± 4	15 ± 3	
Anode carbonate / μmol	8 ± 3	9 ± 2	11 ± 2	

3.2 Effect of Hydration on the Performance of AEMFCs Operating with 400 ppm CO₂

Another variable that may influence the CO₂ uptake in the AEM cell is cell hydration. There are multiple ways to manipulate the amount of water in the cell. One way is to change the dew point of the anode and cathode reacting gases. results of doing so on the CO₂-related voltage loss is shown in Figure 4a and summarized in Table 4. At low to intermediate dew point values, the total CO₂-related overpotential very slightly decreased with increased hydration (evidenced the by the lower HFR in Table 4). As the dew points were increased, the concentration and flux of CO₂ in the anode exhaust decreased while the concentration leaving the cathode increased, shown in Figure 4b-c. This appears to confirm that increasing the amount of free water in the cell slightly lowers CO₂ uptake in the cathode. The presence of this free water most likely leads to a dilution effect, where the environment is made less basic in nature, decreasing the CO₂ solubility. At the highest dew point settings, the total CO₂ overpotential was low, but this was subject to a tradeoff where the high hydration levels led to anode flooding (excess liquid water), which reduced overall cell performance and resulted in fluctuations in the cell voltage (cathode/anode dew points = 55/57 °C in Figure 4a).

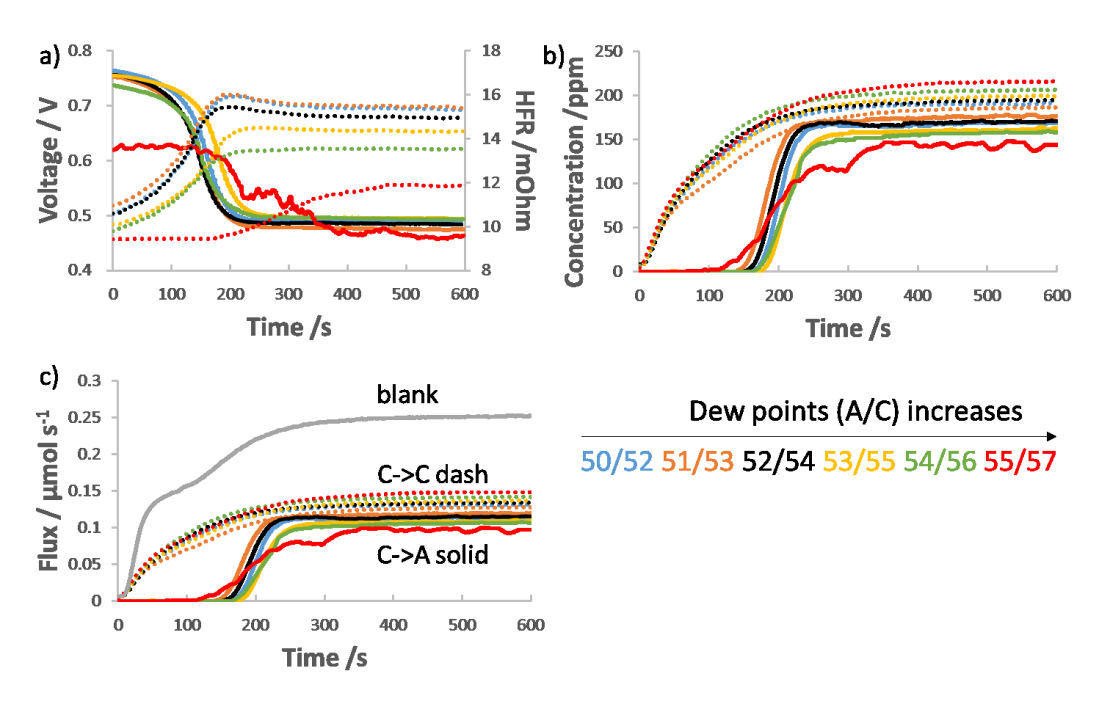


Figure 4. Effect of water content on the carbonation of AEMFCs operating at 1 A/cm^2 and $60 \text{ }^{\circ}\text{C}$ with ETFE-BTMA AEM, 5 cm^2 active area. 400 ppm CO_2 in O_2 was fed to cathode at t = 0 s, and UHP H_2 to the anode, both at a rate of 1 L/min. a) voltage loss and HFR increase as function of dew points (anode/cathode); b) CO_2 emission from the anode (solid lines) and cathode (dotted lines); c) CO_2 flux.

Table 4. Influence of hydration on the CO₂-related overpotential and degree of carbonation for an AEMFC operating at 60 °C.

Anode/Cathode Dew Points	50/52	51/53	52/54	53/55	54/56	55/57
CO ₂ overpotential /V	0.277	0.277	0.272	0.261	0.244	0.151
△HFR / mOhm	4.73	4.43	4.37	4.21	3.72	2.66
AEMFC carbonate / μmol	17 ± 1	16 ± 1	14 ± 1	18 ± 1	15 ± 1	17 ± 1
Anode carbonate / µmol	16 ± 1	15 ± 1	17 ± 1	17 ± 1	17 ± 1	12 ± 1

A second pathway to change the water content of the cell is to manipulate the polymer itself. One way to do that is to vary the amount of water that can be taken up by the polymer, which can be done by changing its degree of crosslinking or the ratio of the monomers in the copolymer. To show this effect, the percentage of crosslinker in a GT-64 polynorbornene copolymer AEM was varied from 5% to 25%. As the degree of crosslinking is increased, the water uptake is reduced. ¹⁰ Therefore, in this study, the GT-64-5 AEM had the highest water content and GT-64-25 had the lowest water content. As shown in Figure 5a, the overall voltage loss decreased with increasing water content. GT-64-5, -15, and -25 AEMFCs showed overall CO₂-related the voltage losses of 254 mV, 292mV, and 300mV, respectively. Figures 4 and 5 confirm that increasing the water contents in an operating AEMFC helps reduce the CO₂-related performance penalty. Figure 5b reports the CO₂ concentrations in the anode and cathode effluents for the GT-64 AEMs with varied crosslinking. Interestingly, the overall amount of CO₂ taken up by the cell does not appear to be significantly changed by the crosslinker content. But, the lower crosslinker content (higher water content) did have a clear effect on the HFR and voltage loss. This suggests that the membrane water can influence the cell behavior even if the total CO₂ content of the cell is similar.

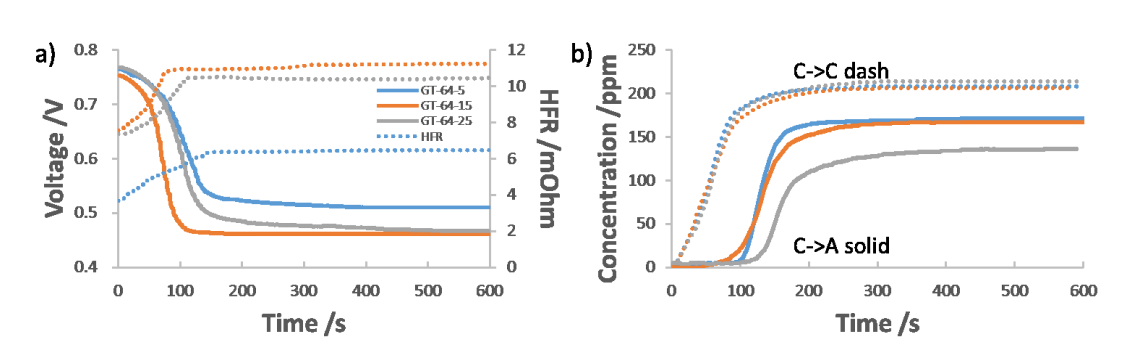


Figure 5. Influence of water uptake on AEMFC carbonation for cells operated at 1 A/cm^2 and $74/74/80 \,^{\circ}\text{C}$ (A/C/cell) with $10 \, \mu\text{m}$ thick GT-64-X AEMs. The GT-64-X AEMs contain increasing crosslinker content (5%, 15%, and 25%, denoted as X = 5, 15, 25, respectively). 400 ppm CO₂ was fed to cathode, 5 cm² active area. Specifically shown are a) voltage loss and HFR increase and b) CO₂ emission from the anode (solid lines) and cathode (dotted lines) as crosslinker content is increases.

3.3 Optimizing operating conditions to minimize the effect of CO₂ on AEMFCs

The results above show that lower cathode flowrate (i.e. high ratio between the anode/cathode flowrate) and higher cell water content both contribute to lower total CO₂-related voltage loss. The experimental results in this work also agree with the modeling work by Gerhardt et al.²³ and Setzler et al.²⁶ who both showed that the degree of carbonation increased with decreased cathode flowrate. In addition to these two mechanisms, our previous work¹⁶ showed that higher operating current density, lower the CO₂ concentration, and higher temperature also lowered CO₂-related voltage losses. Therefore, we deployed a combination of the above advantageous conditions and operated a cell at 80 °C, anode/cathode dew points of 78/80 °C, high anode flowrate at 1L/min and low cathode flowrate at 0.2 L/min. We then recorded point-by-point data with varied CO₂ content in the cathode at a constant current density of 2 A/cm² (Figure 6a). Polarization curves were also recorded at several cathode CO₂ concentrations (Figure 6b).

As shown in Figure 6a, under these "optimized" conditions, operating an AEMFC with low CO₂ concentrations did not lead to catastrophic voltage losses. In fact, only a 30 mV voltage loss was observed with 5 ppm CO₂ in the cathode feed. When 400 ppm CO₂ oxygen was fed to the cathode, the total CO₂-related voltage loss was 182 mV, which is half of the previously reported value, 16 showing that the operating conditions are vitally important in dictating CO₂ tolerance. As the CO₂ concentration exceeded 100 ppm, there was an asymptotic behavior where increasing from 100 ppm to 400 ppm did not significantly affect the CO₂-related voltage losses. However, increasing the concentration of CO₂ in the cathode feed led to further decreases in the achievable mass transport limiting current and peak power density. However, most AEMFCs (like most PEMFCs), would not actually be operated near the peak power density. Considering a more realistic operating point (2 A/cm² at 0.6 V) for various applications, including automotive, there was only ca. 20% reduction in the power density with 400 ppm CO₂ in the cathode gas compared to benchmark CO₂-free conditions. slightly lower concentrations (<100 ppm) have less than a 10% loss. This seems to provide some good news -that AEMFCs can be operated with CO2 in the cathode stream, even at 400 ppm, without catastrophic performance losses. It is important to acknowledge that pure oxygen instead of air is being used here when the latter has reduced overall performance. The focus here is on the intrinsic effect of CO₂, justifying the use of O₂, but it is noted that the use of air is a more realistic operating condition for automotive and other applications.

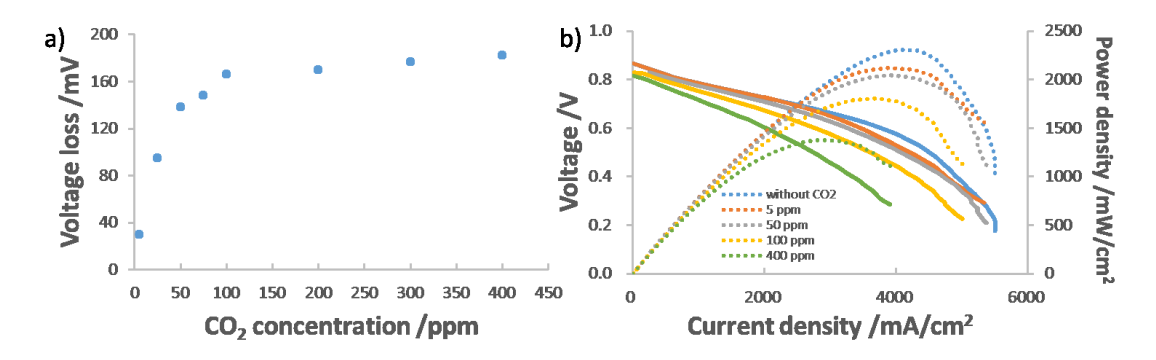


Figure 6. a) Voltage loss as function of CO_2 concentration at 2 A/cm² cell discharge; b) Power density curves for AEMFCs operated at various CO_2 concentrations in O_2 , up to 400 ppm. The cell was operated at 80 $^{\circ}$ C with anode/cathode dew points of 78/80 $^{\circ}$ C. The anode flowrate was 1L/min and the cathode flowrate was 0.2 L/min. The membrane was HDPE-BTMA (ca. 30 μ m thick when fully hydrated). 5 cm² active area.

4. Conclusions

In this study, it experimentally shown in high performance AEMFCs that decreasing the total CO₂ dose to the cell (by decreasing the cathode flowrate) and increasing the level of hydration in an operating AEMFC are two possible pathways to lowering the CO₂-related voltage losses. Considering the fundamental mechanisms for CO₂-related voltage losses, the Nernstian contribution dominated voltage losses and was not affected by the gas flowrates. The next most important contributor to voltage loss was the anode charge transfer resistance, which increased with increasing O₂ flowrate and decreasing H₂ flowrate. The Ohmic resistance increased with increasing cathode flowrate, but was a minor overall contributor to cell performance losses. Lastly, a new set of optimal conditions, which lowered the total CO₂-related overpotentials to achieve practical current-voltage values was found and demonstrated. These insights will help both modeling groups and experimental researchers to better understand the operation

of AEMFCs with CO₂ containing cathode feeds, as well as allow them to pose and assess new solutions.

It is also shown that AEM-like devices may be able to act as CO₂ separators that can simultaneously generate power. Finally, as the anode feed flowrate decreased, the CO₂ concentration in the anode increased to levels several times larger than the cathode inlet concentration, showing that these devices can act as energy-generating CO₂ concentrators.

Acknowledgements

The authors gratefully acknowledge the financial support of the U.S. National Science Foundation (Award Number: 1803189) for the effort expended by Y.Z. and W.E.M. to perform the AEMFC experiments, analyze data and prepare the manuscript. G.H. and P.K. gratefully acknowledge the support of ARPA-E Ionics Program. The AEMs were fabricated using resources provided by UK EPSRC grant EP/M014371/1.

5. References

- G. Merle, M. Wessling and K. Nijmeijer, *J. Memb. Sci.*, 2011, **377**, 1–35.
- 2 E. Gülzow and M. Schulze, *J. Power Sources*, 2004, **127**, 243–251.
- 3 A. Sen A. Tewari, V. Sambhy, M. Urquidi Macdonald, *J. Power Sources*, 2006, **153**, 1–10.
- 4 L. A. Adams, S. D. Poynton, C. Tamain, R. C. T. Slade and J. R. Varcoe, ChemSusChem, 2008, 1, 79–81.

- 5 K. K. V. Cifrain M, J. Power Sources, 2004, 127, 234–242.
- J. A. Vega, C. Chartier and W. E. Mustain, *J. Power Sources*, 2010, **195**, 7176–7180.
- 7 K. N. Grew and W. K. S. Chiu, *J. Electrochem. Soc.*, 2010, **157**, B327.
- P. A. Kohl, G. Huang and M. Mandal, in *The Electrochemical Society Meeting Abstracts*, 2019, vol. 33, pp. 1733–1733.
- 9 L. Wang, J. J. Brink and J. R. Varcoe, *Chem. Commun.*, 2017, **53**, 11771–11773.
- G. Huang, M. Mandal, X. Peng, A. C. Yang-Neyerlin, B. S. Pivovar, W. E. Mustain and P. A. Kohl, *J. Electrochem. Soc.*, 2019, **166**, F637–F644.
- M. Mandal, G. Huang, N. U. Hassan, X. Peng, T. Gu, A. H. Brooks-starks, B. Bahar, W. E. Mustain and P. A. Kohl, *J. Electrochem. Soc.*, 2020, **167**, 054501.
- S. M. Alia, K. Neyerlin, K. Hurst, J. W. Zack, S. A. Mauger, W. W. McNeary,
 A. Weimer, W. Medlin, S. Zaccarine, C. Ngo, S. Pylypenko, K. Buechler and
 B. S. Pivovar, in *The Electrochemical Society Meeting Abstracts*, 2018, vol. 44,
 pp. 1505–1505.
- S. M. Alia, S. Stariha, R. L. Borup and B. S. Pivovar, in *The Electrochemical Society Meeting Abstracts*, 2018, vol. 46, pp. 1604–1604.
- W. E. Mustain, in *The Electrochemical Society Meeting Abstracts*, 2018, vol.47, pp. 1637–1637.
- T. J. Omasta, X. Peng and W. E. Mustain, in *The Electrochemical Society Meeting Abstracts*, 2018, vol. 30, pp. 1754–1754.

- Y. Zheng, T. J. Omasta, X. Peng, L. Wang, J. R. Varcoe, S. Pivovar and W. E. Mustain, *Energy Environ. Sci.*, 2019, 12, 2806–2819.
- Z. Siroma, S. Watanabe, K. Yasuda, K. Fukuta and H. Yanagi, *ECS Trans.*,2010, 33, 1935–1943.
- 18 Y. Matsui, M. Saito, A. Tasaka and M. Inaba, ECS Trans., 2010, 25, 105–110.
- M. Inaba, Y. Matsui, M. Saito, A. Tasaka, K. Fukuta, S. Watanabe and H. Yanagi, *Electrochemistry*, 2011, **5**, 322–325.
- 20 H. Yanagi and K. Fukuta, ECS Trans., 2008, 16, 257–262.
- W. A. Rigdon, T. J. Omasta, C. Lewis, M. A. Hickner, J. R. Varcoe, J. N. Renner, K. E. Ayers and W. E. Mustain, *J. Electrochem. Energy Convers.*Storage, 2017, 14, 1–8.
- M. R. Gerhardt, L. M. Pant, H.-S. Shiau and A. Z. Weber, *ECS Trans.*, 2018,86, 15–24.
- M. R. Gerhardt, L. M. Pant and A. Z. Weber, *J. Electrochem. Soc.*, 2019, 166,
 F3180–F3192.
- U. Krewer, C. Weinzierl, N. Ziv and D. R. Dekel, *Electrochim. Acta*, 2018,263, 433–446.
- J. A. Wrubel, A. A. Peracchio, B. N. Cassenti, T. D. Myles, K. N. Grew and W. K. S. Chiu, *J. Electrochem. Soc.*, 2017, 164, F1063–F1073.
- B. P. Setzler and Y. Yan, in *The Electrochemical Society Meeting Abstracts*, 2017, vol. 01, p. 1654.
- J. A. Wrubel, A. A. Peracchio, B. N. Cassenti, K. N. Grew and W. K. S. Chiu,

- J. Electrochem. Soc., 2019, 166, 810-820.
- 28 B. P. Setzler, L. Shi, T. Wang and Y. Yan, in *The Electrochemical Society Meeting Abstracts*, 2019, vol. 34, p. 1824.
- T. J. Omasta, A. M. Park, J. M. Lamanna, Y. Zhang, X. Peng, L. Wang, D. L. Jacobson, J. R. Varcoe, D. S. Hussey, B. S. Pivovar and W. E. Mustain, *Energy Environ. Sci.*, 2018, 11, 551–558.
- T. J. Omasta, L. Wang, X. Peng, C. A. Lewis, J. R. Varcoe and W. E. Mustain, J. Power Sources, 2017, 205–213.
- 31 L. Wang, J. J. Brink, Y. Liu, A. M. Herring, J. Ponce-González, D. K. Whelligan and J. R. Varcoe, *Energy Environ. Sci.*, 2017, 10, 2154–2167.
- L. Wang, E. Magliocca, E. L. Cunningham, W. E. Mustain, S. D. Poynton, R. Escudero-cid, M. M. Nasef, J. Ponce-gonzález and R. Bance-souahli, *Green Chem.*, 2017, **19**, 831–843.
- 33 L. Wang, X. Peng, W. E. Mustain and J. R. Varcoe, *Energy Environ. Sci.*, 2019, **12**, 1575–1579.